Journal of Applied Polymer Science

Perfluorinated Lubricant/ Polypyrrole Composite Material: Preparation and Corrosion Inhibition Application

Hongfei Zhu,[1,2] Jian Hou,[2] Ri Qiu,[2] Jiong Zhao,[2] Jingkun Xu[1]

[1]Jiangxi Key Laboratory of Organic Chemistry, Jiangxi Science & Technology Normal University, Nanchang 330013, People's Republic of China

[2]Science and Technology on Marine Corrosion and Protection Laboratory, Luoyang Ship Material Research Institute, Qingdao 266101, People's Republic of China

Correspondence to: J. Xu (E-mail: xujingkun@tsinghua.org.cn)

ABSTRACT: Chronoamperometry technique was used to prepare polypyrrole onto low alloy steel surface from aqueous solutions. The morphology and composition of the as-obtained deposit was characterized by scanning electron microscopy, X-ray diffraction, and Fourier-transform infrared techniques. The dendritic polymer could be realized at the high potential and favorable mass transfer conditions. Contact angle tests proved that the polypyrrole with rough surfaces had small contact angles. After the modification with the 1H, 1H, 2H, 2H-perfluorooctyl trichlorosilane, the values of contact angles of polypyrrole reached up to *ca.* 130°. The consequent infusion of perfluorinated lubricant into the hydrophobic matrix led to a composite material. Potentiodynamic polarization tests in 3.5 wt % NaCl solution revealed that low alloy steel covered with this composite material raised the corrosion potential more than 1000 mV and decreased the corrosion current density *ca.* 3 orders, suggesting that the perfluorinated lubricant/ polypyrrole composite material behaved as a good candidate for corrosion inhibition. © 2013 Wiley Periodicals, Inc. J. Appl. Polym. Sci. **2014**, *131*, 40184.

KEYWORDS: coatings; electrochemistry; composites

Received 27 January 2013; accepted 12 November 2013
DOI: 10.1002/app.40184

INTRODUCTION

Nowadays, conducting polymers of micro- or nano-scale have been intensively investigated because of their interesting and unexpected properties.[1–4] As a conventional and typical conducting polymer, polypyrrole (PPy) is particularly attractive because of its highly environmental stability and easy preparation in aqueous solution.[5] In metal corrosion and protection field, PPy can be deposited onto the metal surface and behave as a barrier to block the invasion of H_2O, Cl^-, and oxygen from the external environment, so that much attention has been paid to develop PPy as a corrosion inhibition coating on numerous metal surfaces.[5–8] Annibaldi reported that adherent and homogeneous PPy coating was electrodeposited on copper from a salicylate solution.[9] The polymer coating remained stable after the immersion in 0.6*M* NaCl aqueous solution for more than 2 weeks. Saidman and coworker found that the PPy had good properties of adhesion and corrosion protection so that it could efficiently decrease the pitting corrosion of 316L stainless steel.[7] Tüken et al. investigated PPy films modified by graphite, which exhibited a good coating performance to stainless steel by hindering the attack from corrosive environment.[10] In previous research of our group, it was found that the addition of phosphotungstic acid to PPy could increase its corrosion protection efficiency for the low alloy steel in seawater.[11] Although many progresses have been made in previous studies, some intrinsic problems, e.g., the corrosion inhibition efficiency and sustainability, are still nagging its future development and practical application.

Currently, the phenomenon of superhydrophobicity and the preparation of synthetic superhydrophobic surfaces have been intensively investigated because of their potentially industrial and biomedical applications.[12–14] According to Cassie–Baxter theory,[15,16] the surface morphology, roughness, and chemical composition act as the main roles to determine the surface wettability. Applying the superhydrophobic layer as corrosion inhibition barrier has been proven as a new strategy for metal protection. In previous studies, researchers have demonstrated that superhydrophobicity can confer corrosion inhibition capabilities to metals such as steel, Zn, Al, Cu, and others .[17–25] For the short time immersion during the corrosion capability evaluation, the superhydrophobicity layer can temporarily behave as good cushion to protect the underneath metal from corrosion.

However, the superhydrophobic matrix is far away from optimal. For instance, using the superhydrophobicity as the corrosion inhibition barrier, the surface still cannot hinder the attack from the corrosive environment for long time, and the ions and water will penetrate through the failed superhydrophobic layer to reach the underlying metal substrate. The corrosion will consequently occur.[24] It is urgent to develop more sophisticated and novel material to combat the corrosion exerted from the external environment.

Recently, inspired by Nepenthes plant in nature, Aizenberg and coworkers have reported a new style of compositing material with the slippery liquid-infused porous surface (SLIPS). The compositing of this material is as follows: firstly, a micro/nanoscale rough surface is fabricated; after that, the as-formed rough surface is modified by the fluoride agent, so that a strongly hydrophobic surface having high affinity to oil will be achieved. Lubricant fluid is externally injected onto the porous surface. The existing micro/nanopores will exert strong capillary force to the infused fluid, and a liquid film is firmly anchored onto the surface. SLIPS shows extremely excellent self-healing, anti-icing, and antifrosting performances.[26,27] What surprises the experts working on material protection fields most is the extraordinary antifouling properties from SLIPS, as the fouling from bioorganisms is another source causing severe deterioration to metal materials. SLIPS behaves much better antifouling feature (*ca.* 35 times the reduction of attached biofilm) than the best case scenario, state-of-the-art PEGylated surface, so that SLIPS can be regarded as having exceptional anti-biofouling performance.[28] Metals immersed underwater endure both fouling and corrosion to shorten the longevity. If SLIPS can also perform enhanced corrosion inhibition property to metals, this new category of material can be regarded to have both anticorrosion and antifouling properties.

Herein, we apply SLIPS as the surface coating to protect low alloy steel from the corrosion. During the PPy matrix electrodeposition process, different morphologies are obtained when applying different potentials. Motivated by the relatively high deposition potential, the dendritic polymer can be accomplished, and the formation of this morphology is highly determined by the electrode geometry. With the infusion of the lubricant, the SLIPS composite material is achieved. It is anticipated that the SLIPS can potentially act as a new promising candidate for corrosion inhibition.

EXPERIMENTAL

PPy/LS Samples Preparation

The substrate for PPy electrodeposition was Ni–Cr low alloy steel, which was cut into 1 cm×1 cm samples and sealed in epoxy resin as working electrodes. The sample surfaces were polished using SiC abrasive paper (1500 grit). After the grinding, they were degreased with acetone and washed with deionized water, respectively. The as-prepared steel was used as the substrate for PPy to grow.

All electrochemical experiments were carried through on an ACM electrochemical platform (Gill AC). Electrochemical growth of PPy were performed in a typical three-electrode cell, in which the low alloy steel, platinum–niobium wire and saturated calomel electrode (SCE) were used as working, counter, and reference electrode, respectively. If there is no specific indication, all the potentials in this manuscript are reported taking SCE as the reference. Pyrrole (C. P. Sinopharm) aqueous solution with the concentration of 0.2*M* was prepared using 0.1*M* sodium dodecyl sulfate (A. R. Sinopharm) as the supporting electrolyte. After growing at different potentials (1.0, 1.4, 1.8, and 2.2 V) for 900 s in the mixed solution, PPy was deposited on low steel surface (denoted as PPy/LS). The as-obtained PPy/LS samples were rinsed with water to remove the remaining solution and then dried under a stream of nitrogen for further characterization. Surface morphology analysis of the deposited films was performed on an environment scanning electron microscope (ESEM, Philips XL 30). The phase composition of the deposit was studied by X-ray diffraction (XRD, Bruker D8 Advance). The structure of PPy film was further characterized by Fourier-transform infrared spectrophotometer (FT-IR, Nicolet 8700). Before this characterization, the PPy film was peeled off from PPy/LS and dissolved in acetone for 1 h. The solution was dropped onto the surface of KBr pellet for the characterization.

Formation of Perfluorinated Lubricant/PPy/LS

The formation of PFL/PPy/LS was realized by following the route reported in previous study.[27] Firstly, 1H, 1H, 2H, 2H-perfluorooctyl trichlorosilane (Aldrich) was dipped onto the as-prepared PPy films, which were stored in a desiccator for 24 h to form a hydrophobic surface (named as M-PPy/LS). After that, the M-PPy/LS was infused with a perfluorinated lubricant, perfluoroalkylether (Nascent FX 6200, Du Pont), to form perfluorinated lubricant/PPy/LS (denoted as PFL/PPy/LS). The wettability properties of the as-prepared materials such as PPy and M-PPy/LS were measured with a contact angle meter (CAM-101, KSV Instruments). The water droplet used for the measurement was adopted *ca.* 3 μL.

The corrosion performance of different materials was tested in a 3.5 wt % NaCl aqueous solution, and the samples included LS,

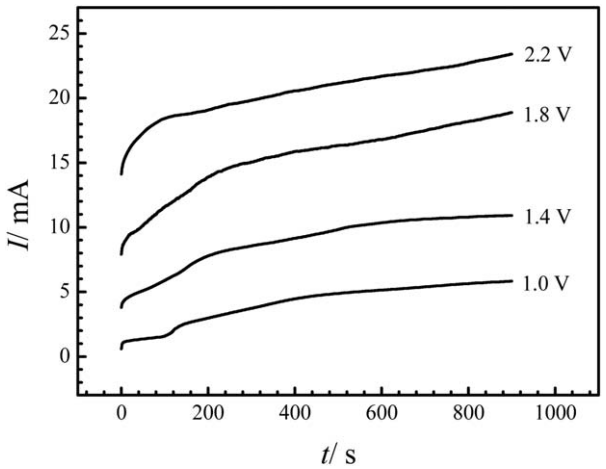

Figure 1. *I–t* plots during electrochemical deposition of PPy onto low alloy steel at different potentials.

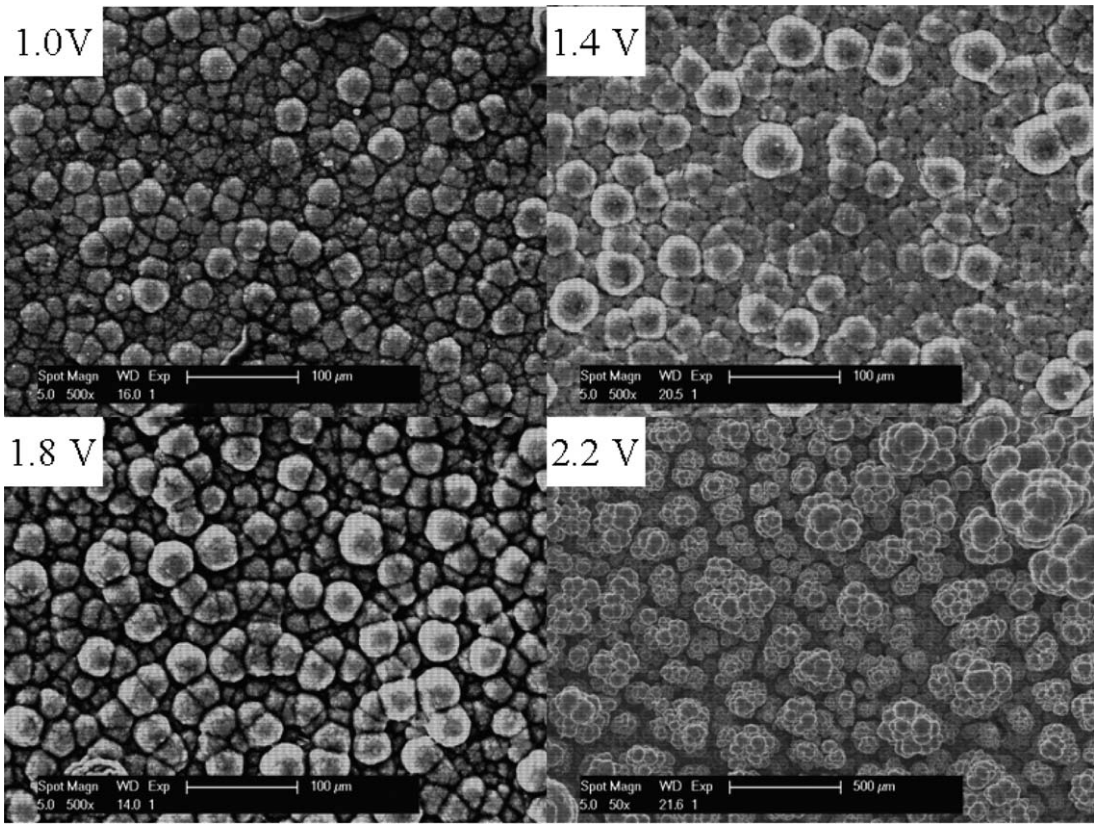

Figure 2. SEM images of microstructure of PPy films obtained at different deposition potentials. The electrolysis time was 900 s for each sample preparation.

PPy/LS, and PFL/PPy/LS. The potentiodynamic tests were carried out with a 1 mV/s scanning rate in the range of ± 0.500 V offset of the open circuit potential. Electrochemical impedance spectroscopy was achieved by a Model 283 potentiostat/galvanostat (EG&G Princeton Applied Research). The corrosion morphology of the different materials immersed in NaCl solution was checked with a Hirox 8700 optical microscopy.

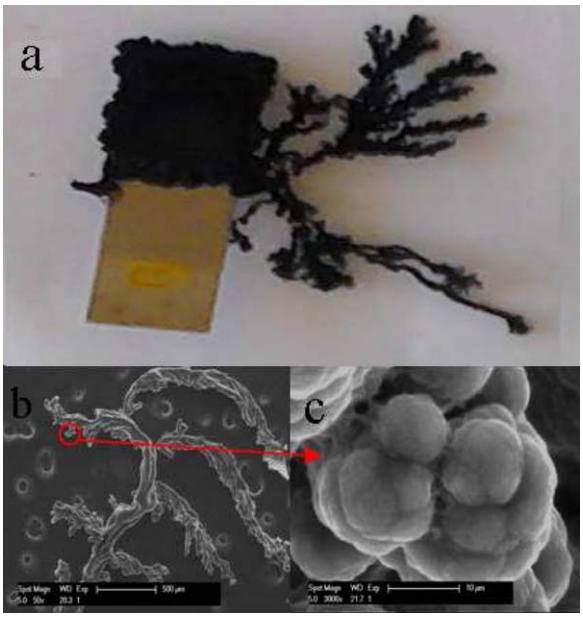

Figure 3. The photo (a) and ESEM (b, c) images of dendritic PPy morphology on a 304 stainless steel foil. The electrodeposition was realized at 2.2 V for 900 s. [Color figure can be viewed in the online issue, which is available at wileyonlinelibrary.com.]

RESULTS AND DISCUSSION

Electrochemical Synthesis of PPy at Different Potentials

In previous reports, the conventional potential for the electrochemical deposition of PPy was 0.75–1.0 V in various aqueous

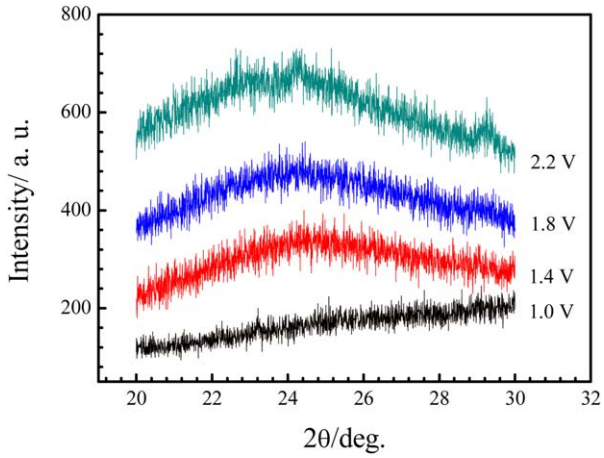

Figure 4. X-ray diffraction of the samples formed at different deposition potentials. [Color figure can be viewed in the online issue, which is available at wileyonlinelibrary.com.]

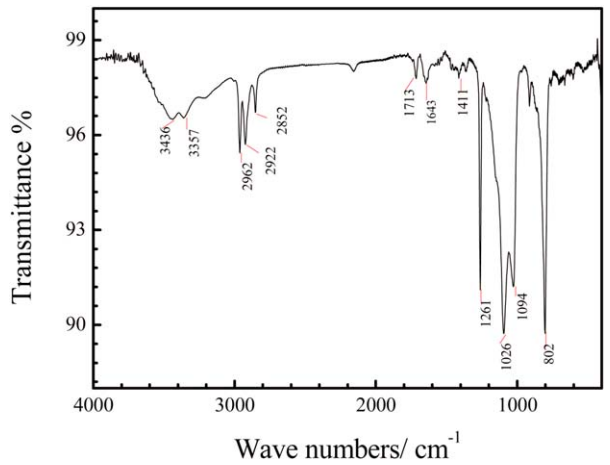

Figure 5. FT-IR spectra of the PPy film obtained at 1.8 V with 900 s electrodeposition time. [Color figure can be viewed in the online issue, which is available at wileyonlinelibrary.com.]

solutions.[5,27,29] Qiu et al. investigated that overpotential could induce rough structures, e. g., dendritic structure,[30–32] and the rough structure could show versatile functions because of the large roughness and surface area. It is believed that the high motivation during the metallic material growth process will enable the fractal and dendritic morphology growth. For the conducting polymer, i.e., the synthetic metal, the electrodeposition process is similar to that of the metal, except that the polymer monomer has much larger size than single metal atom. The aggregation of the monomer to a deposit is often realized by the electrochemical oxidation route. However, for the metal electrodeposition, the electrochemical reduction is often applied to the "welding" of the metal atoms. In this report, the pyrrole monomer is chosen as the candidate to illustrate the electrochemical motivation to impact the resulting polymer morphology. Several high electrochemical deposition potentials, e.g., 1.0, 1.4, 1.8, and 2.2 V, have been used to enforce PPy to grow. The *I–t* plots obtained during the electrochemical synthesis at different applied potentials are shown in Figure 1. It is observed that the current of all plots show the increasing tendency during the electrolysis process, which is similar to the scenario when electrodepositing metal/alloy from the salt solutions.[30,31] Generally, the fractals or dendrites can be formed on the electrode surface when the motivation is large. The new coming monomers will be oxidized and attached to the tips of the fractals to realize the elongation, and the refreshed fractals will consequently act as the electrode in the sequential deposition process. The working electrode is actually an "alive" one instead of an electrode with fixed area. As the process going on the electrode area will be getting larger, and the fractal tips will be growing longer. In turn, they can penetrate the primary double layer to reach new fresh feed stock to achieve more monomers to supply the further growth. The larger electrode area and larger concentration will result in the larger current as recognized from Figure 1. Moreover, it is observed that the higher applied potential has the larger polymerization motivation, which in turn enforces the higher current value. The potential works as the key parameter to determine the electrochemical behavior during the electrodeposition process.

Figure 2 show the SEM images of the PPy films prepared at different potentials. Obviously, for the potentials of 1.0, 1.4, and 1.8 V, the films are mainly composed by the granules, and there is no significant difference among them. The PPy polymer is observed as small spherical grains and the average size reaches tens of microns. However, when the potential is afforded as 2.2 V, the morphology has dramatic change. Instead of the typical round granule, the ramified hierarchical fractal can be formed on an embedded steel substrate. Using a foil electrode, the dendritic structure can be formed in the edge area of the electrode at the same electrodeposition potential (Figure 3). As the edge of the foil has an opening geometry larger than the embedded electrode, there is the larger mass transport in the edge than the inner part, which enforces the formation of the dendritic structure. Based on this truth, it is proved that the conducting polymer having dendritic morphology can also be achieved by the electrodeposition process, and the dendritic structure is a ubiquitous phenomenon accompanying with the electrodeposition process, no matter the deposition substance is the metal, alloy, or the synthetic metals, i.e., conducting polymers. The formation of the dendritic polymer can also be determined by the parameters, such as potential, mass transfer, and so forth. Nevertheless, compared with metals and alloys, the conducting

Table I. Peaks and the Corresponding Vibration Groups of the PPy Film Formed at 1.8 V Potential in FTIR Spectra

Peaks/cm^{-1}	3436, 3357	2962, 2922, 2852, 802	1713, 1643, 1411	1261, 1094, 1026
Functional group	Stretching vibration —N—H	—C—H Vibration	Stretching vibration C=C	Stretching vibration C—N

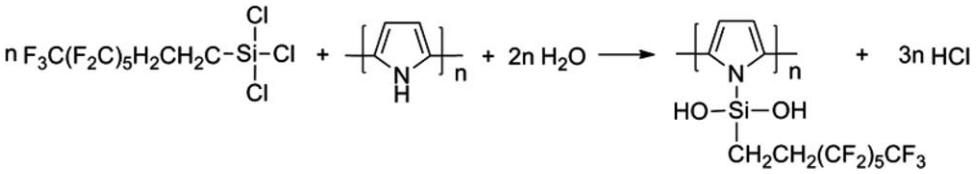

Scheme 1. Modification of PPy with 1H, 1H, 2H, 2H-perfluorooctyl trichlorosilane in ambient environment.

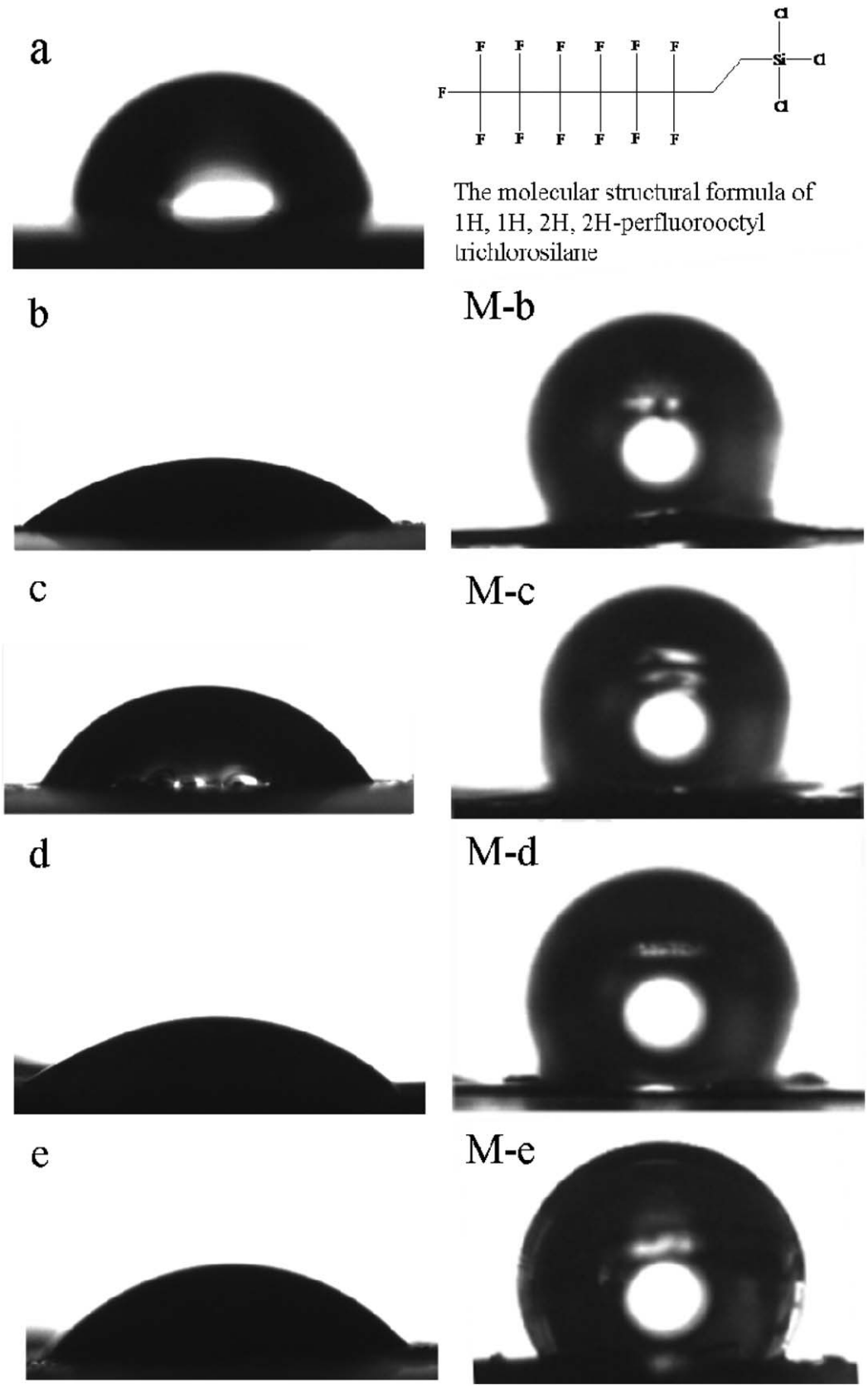

Figure 6. (a) Contact angles images of LS. (b–e) the contact angle of PPy/LS, in which the PPy film was electrodeposited at 1.0, 1.4, 1.8, and 2.2 V, respectively. After the modification by 1H, 1H, 2H, 2H-perfluorooctyl trichlorosilane, the corresponding contact angle scenario was shown as M-b, M-c, M-d, and M-e.

polymer dendrite has its own intrinsic property. As it is noncrystalline structure, there is no favorable direction during the growth process, so that the external appearance seems irregular.

The X-ray diffraction has confirmed the noncrystalline phase of PPy. As shown in Figure 4, the broad bumps detected at *ca.* 24° indicate the low crystallinity of PPy matching the report from Chougule et al.,[33] which is caused by the strong interaction within the polymer matrix. Ouyang et al. reported that the phenomenon was mainly because of the scattering from PPy chains at the interplanar spacing.[34,35] However, the spike peaks cannot be observed in the pattern, which indicates that there is no long-range order existing in the polymer. Figure 5 shows the FT-IR absorption spectrum of PPy films obtained at the deposition potential of 1.80 V. N–H stretching vibration band of PPy ring appear at 3357–3436 cm^{-1} while the characteristic peaks at 1713, 1643, and 1411 cm^{-1} correspond to the C=C stretching. Other peaks related to different vibrations are outlined in Table I. With the characterization by XRD and IR, it is confirmed that the electrodeposition realizes the PPy formation on the electrode surface.

Because the as-obtained PPy typically behaves the rough topography, there are many gaps around the granular PPy with the scale of micrometer, which can steadily induce large capillary force to occur. The aqueous phase will be easy to penetrate into the gaps so that the dissolved corrosive species such as chloride can reach the underlying metal surface, and the corrosion will not be avoided. The surface hydrophobilization is a facile route for the surface to get rid of this inferiority. Hydrophobic agent 1H, 1H, 2H, 2H-perfluorooctyl trichlorosilane was used to modified the structure of PPy films in order to induce hydrophobic and oil-loving surfaces that could admit the infused perfluorinated lubricant, which is expected to act as an effective corrosion inhibition barrier. The reaction between PPy and 1H, 1H, 2H, 2H-perfluorooctyl trichlorosilane is shown as Scheme 1. The Si–Cl will react with N–H in PPy to form N–Si bonding in the conductive polymer. After that, the hydrophobic segment will be anchored on the polymer surface. The wettability properties of initial and as-modified PPy films are shown as Figure 6, and the respective contact angles are listed in Table II. The contact angle of the bare steel is 83.95°, which is a typical hydrophilic surface. After the PPy deposition, the contact angles of a drop of water on PPy films are around 30°. In previous study, the static contact angle of the relatively flat PPy surface is *ca.* 69.1°,[36] which can be assumed as the intrinsic Young contact angle. According to Wenzel equation $\cos\theta_W = r\cos\theta_Y$, the surface roughness is calculated as 2.43, indicating the unsmooth surfaces of PPy films formed at relatively high potentials.[37] After the modification by the fluorinating agent, contact angle values of surfaces for PPy films increase to 120–130°, suggesting remarkable surface property change. The values are a little lower than 150°, which is the critical value of superhydrophobicity. The surface modification realizes the wettability transformation from hydrophilicity to hydrophobicity, as the organic fluorine tails show the oleophilic property. In addition, the surface is intrinsically porous, so that the surface can accommodate the infused lubricant. The porous structure is regarded as the capillary channel net with the diameter of micro/nanoscale. The capillary force induced will firmly clinch the infused fluid, and the out layer of the fluid can also be anchored to the inner layer to avoid the free flowing, as the van der Waals force of the large molecules is large. With the infusion of the lubricant, the composite material composed by the stationary PPy and lubricant is formed.

Table II. Contact Angles of PPy/LS and the Films Tethered with 1H, 1H, 2H, 2H-Perfluorooctyl Trichlorosilane

Samples	Electrodeposition Potential (V)	Contact Angles (°)
LS	-	83.95
PPy/LS	1.0	22.60
	1.4	34.08
	1.8	21.89
	2.2	30.74
M-PPy/LS	1.0	130.03
	1.4	120.44
	1.8	128.84
	2.2	127.64

Corrosion Inhibition Evaluation

In the composite material, the matrix PPy film will inherently work as the corrosion inhibitor for the underneath metal. The lubricant in the gaps of the matrix is immiscible with water, so that the corrosion species dissolved in the water cannot penetrate this organic barrier to reach the metal surface. With the both effects from PPy and lubricant, it is expected that the composite material can effectively release the corrosion exerted by the external environment. The Tafel plots of LS, PPy/LS and PFL/PPy/LS samples exposed in a 3.5 wt % NaCl solution are presented in Figure 7. Compared to LS having the corrosion potential at *ca.* −950 mV, it is illustrated that the corrosion potentials of all PPy/LS samples have large positive shift to reach *ca.* −400 mV, which suggests that the coating of PPy can significantly change the property. After the infusion of the lubricant, the as-achieved PFL/PPy/LS performs more positive shift of the corrosion potential, which locates at the range of 50–190 mV, depending on the electrodeposition potential. Corrosion currents I_{corr} and linear polarization resistance are also listed to evaluate properties and characteristics for corrosion inhibition as shown in Table III. Obviously, the values of I_{corr} for PPy/LS are almost one order of magnitude lower than that of LS. Attached on the steel, PPy can act as a physical barrier to reduce the diffusion rate of ions and water to the underneath metal. In addition, as a conjugated conducting polymer, existence of unsaturated bonds, –NH polar groups in the PPy functions as anodic inhibitor, which resulted in enhancing the corrosion resistance of the steel.[38]

From the Tafel plots and the parameters values listed in Table III, it is illustrated that PFL/PPy/LS shows good corrosion inhibition property to the underlying LS. The protection efficiency of SLIPS to LS can be larger than 99%. Compared with bare

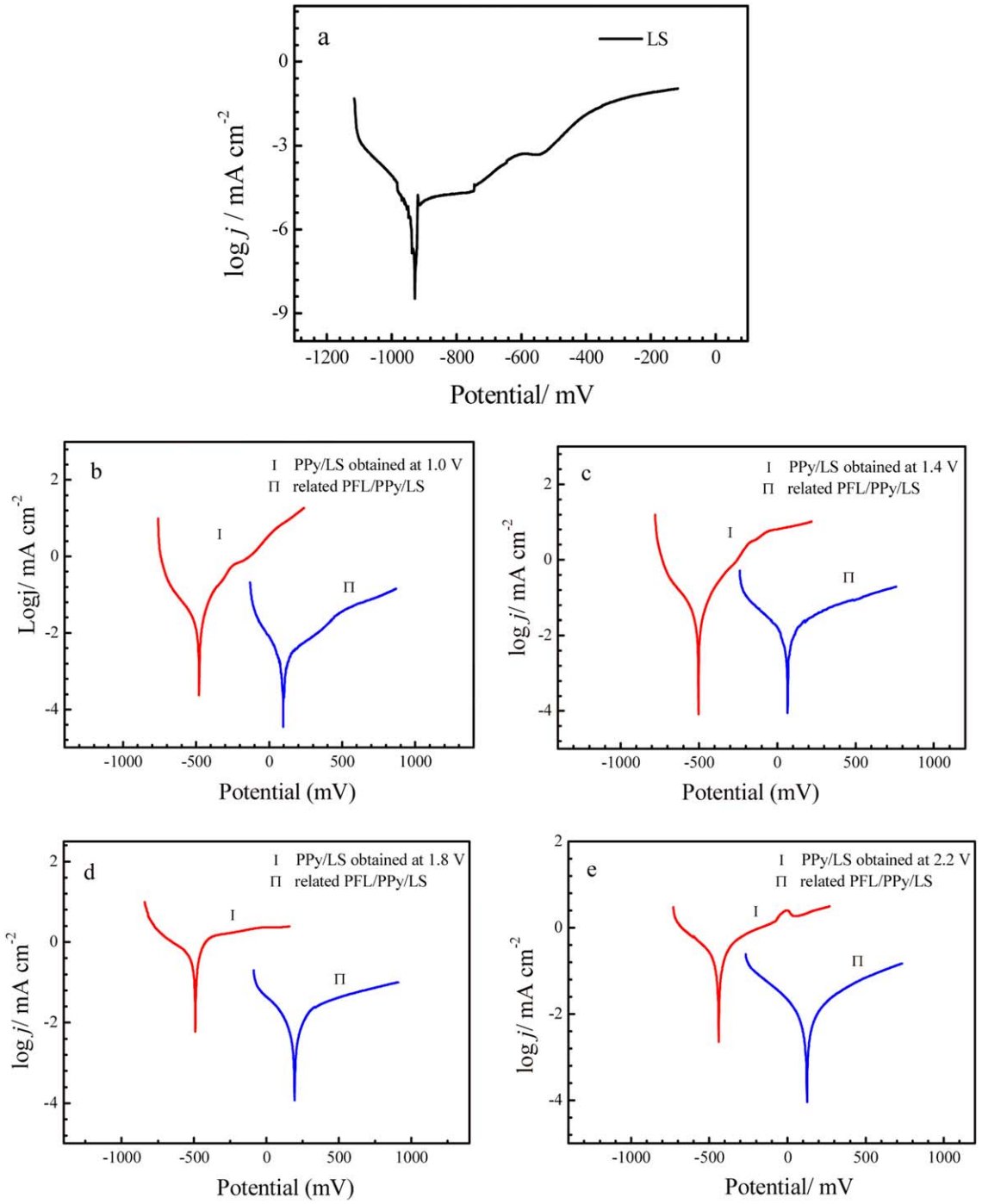

Figure 7. (a) Potentiodynamic polarization plot of LS; (b–e) potentiodynamic polarization behavior comparison between PPy/LS and relative PFL/PPy/LS. [Color figure can be viewed in the online issue, which is available at wileyonlinelibrary.com.]

LS, the corrosion potential has shifted positively more than 1000 mV. I_{corr} has decreased from 4.99 to 3.5 × 10^{-3} mA/cm^2. Moreover, by giving comparison to PFL/PPy/LS and PPy/LS, the positive shift of corrosion potential reaches *ca.* 500 mV, and I_{corr} decreases to *ca.* two orders of magnitude smaller than that of PPy/LS. It can be concluded that PPy/LS has a great improvement of corrosion inhibition performance after the modification by fluorinating agent and covered with perfluorinated lubricant. For the long-term corrosion protection from PFL/PPy, open circuit potential (E_{oc}) and optical microscopy were used to monitor the corrosion state from the corrosive medium. As shown in Figure 8, E_{oc}–t plots reveal that PPy/LS and LS behave similar value during the whole immersion process, i.e., E_{oc} locates at *ca.* −700 mV. As it is hard to achieve a compact conductive polymer on LS surface, there is the direct contact between the underneath LS and solution. However,

Table III. Icorr, Protection Efficiency and Linear Polarization Resistance of LS, PPy/LS and PFL/PPy/LS Samples

Samples	Potentional for getting PPy (V)	I_{corr} (mA/cm^2)	Protection efficiency (%)	Polarization resistance (Ω·cm^2)
LS		4.99		8.90
PPy/LS	1.0	0.33	93.3868	78.06
	1.4	0.34	93.1864	77.00
	1.8	0.15	96.994	170.37
	2.2	0.11	97.7956	235.52
PFL/PPy/LS	1.0	0.0035	99.9299	7558.5
	1.4	0.0059	99.8818	4385.1
	1.8	0.0037	99.9259	7008.8
	2.2	0.0051	99.8978	5074.9

PE = $(I_{corr,\ bare} - I_{corr,\ coated})/I_{corr,\ bare} \times 100\%$, where $I_{corr,\ bare}$ and $I_{corr,\ coated}$ are the corrosion current density for uncoated and coated LS, respectively

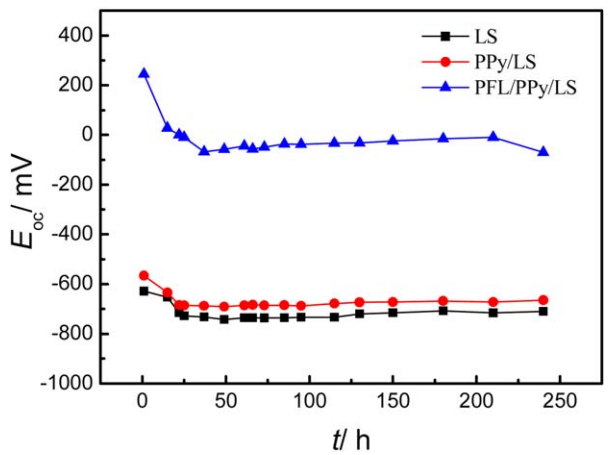

Figure 8. Open circuit potential change during the immersion of the electrode LS, PPy/LS, and PFL/PPy/LS. [Color figure can be viewed in the online issue, which is available at wileyonlinelibrary.com.]

E_{oc} of PFL/PPy/LS behaves differently compared to bare LS and PPy/LS, and its value is near to 0 mV in the long run. Since PPy is not ideally compact, PFL lubricant will flow into the cavities or pores inside of the coating, so that the direct contact between the underneath LS and solution will be isolated. The corrosion protection property from PFL/PPy is substantially enhanced, as shown in Figure 9. Distinguishable corrosion occurs on bare LS after immersion for 20 h. For PPy/LS, after immersion for 140 h, the yellowish product appears on the surface, indicating the corrosion of LS. In short immersion time, PPy can inhibit the corrosion of the underneath metal; however, for the long run, the protection efficiency is limited. Compared with PPy/LS and LS, PFL/PPy exhibits the higher corrosion protection for LS. After immersion for 300 h, the surface still remains stable, indicating LS is efficiently protected by the coating. As schematically shown in Figure 10, oxygen and Cl^- dissolved in the aqueous phase cannot invade into the metal surface, because the lubricant works as the barrier to block the

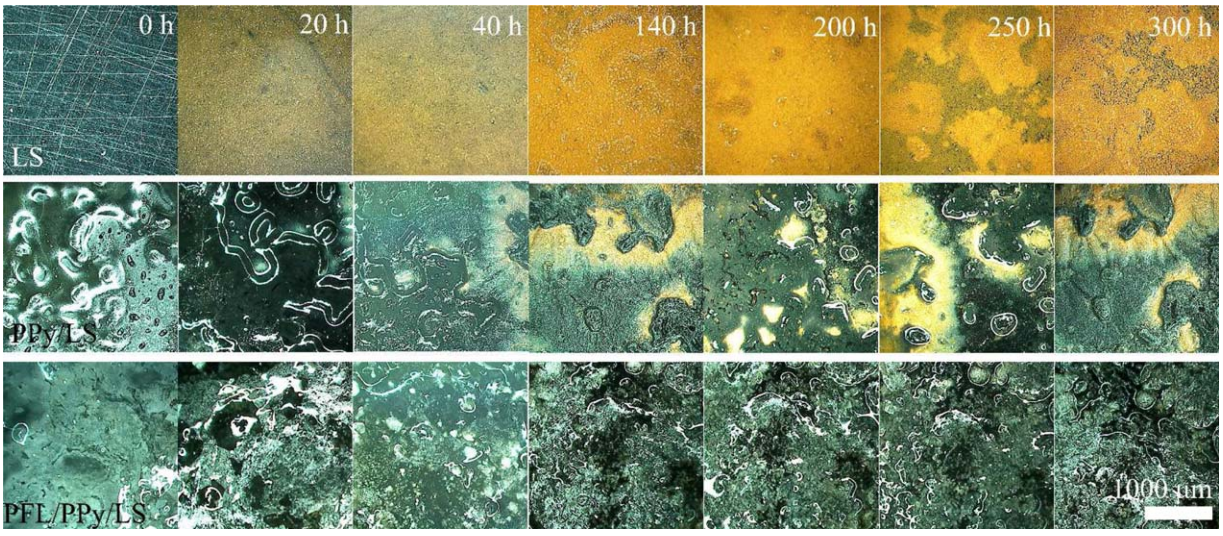

Figure 9. The corrosion status of the different electrodes including LS, PPy/LS, and PFL/PPy/LS in 3.5% NaCl solution. [Color figure can be viewed in the online issue, which is available at wileyonlinelibrary.com.]

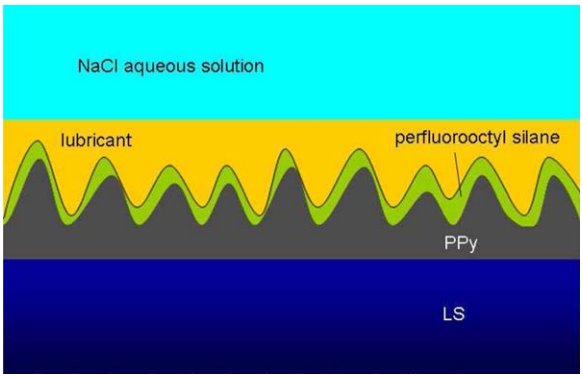

Figure 10. The schematic illustration of corrosion inhibition from the composite material. [Color figure can be viewed in the online issue, which is available at wileyonlinelibrary.com.]

diffusion of the species. As the category of materials can behave as an amazing antifouling coating to prevent the biofouling to occur on the surface, this material can be a potential candidate to work as the antifouling and anticorrosion coating for the metal serving in the marine environment. Much attention is still needed for the fundamental research to understand this coating system, e.g., the diffusion rate of the corrosive species. Further research will be processed in our lab.

CONCLUSIONS

The electrodeposition of PPy onto low alloy steels is successfully carried out using the potentiostatic method in aqueous solutions. The high potential motivates the fractal morphology formation. When the electrode adopts foil geometry, the dendritic morphology will be formed near the edge. However, for a sealed electrode, the fractals instead of the dendritic structure cannot be realized as the mass transfer is not favorable for this morphology formation. The as-modified rough PPy enables the infusion of the lubricant to form a composite material including heterogeneous phases. The composite material behaves good corrosion inhibition for the underlying steel.

ACKNOWLEDGMENTS

This work was supported by the National Science Foundation of China (Grant No. 51073074).

REFERENCES

1. Kim, P.; Epstein, A. K.; Khan, M. *Nano Lett.* **2011**, *12*, 527.
2. Groenendaal, B.; Zotti, G.; Aubert, P. H.; Shane, M. *Adv. Mater.* **2003**, *15*, 855.
3. Olga, B.; Zia, U. K.; Abdellah, M. *Nat. Mater.* **2011** *10* 429.
4. Nie, G. M.; Qu, L. Y.; Xu, J. K.; Zhang, S. S. *Electrochim. Acta* **2008**, *53*, 8351.
5. Flamini, D. O.; Saidman, S. B. *Corros. Sci.* **2010** *52* 229.
6. Zeybek, B.; Pekmez, N. Ö.; Kılıç, E. *Electrochim. Acta* **2011**, *56*, 9277.
7. González, M. B.; Saidman, S. B. *Corros. Sci.* **2011**, *53*, 276.
8. Ryu, H.; Sheng, N.; Ohtsuka, T. *Corros. Sci.* **2012**, *56*, 67.
9. Annibaldi, V.; Rooney, A. D.; Breslin, C. B. *Corros. Sci.* **2012** *59* 179.
10. Tüken, T.; Yazici, B.; Erbil, M. *Surf. Coat. Tech.* **2007**, *202*, 425.
11. Hou, J.; Zhu, G.; Zheng, J. Q. *Polym. Sci. Ser. B* **2011**, *53*, 546.
12. Feng, X. J.; Jiang, L. *Adv. Mater.* **2006**, *18*, 3063.
13. Blossey, R. *Nat. Mater.* **2003**, *2*, 301.
14. Li, X. M.; Reinhoudt, D.; Crego-Calama, M. *Chem. Soc. Rev.* **2007**, *36*, 1350.
15. Cassie, A. B. D.; Baxter, S. *Trans. Faraday Soc.* **1944**, *40*, 546.
16. Baxter, S.; Cassie, A. B. D. *J. Text Ind.* **1945**, *36*, T67–90.
17. Boisier, G.; Lamure, A.; Pébère, N.; Portail, N.; Villatte, M. *Surf. Coat. Tech.* **2009**, *203*, 3420.
18. Gnedenkov, S. V.; Sinebryukhov, S. L.; Egorkin, V. S.; Mashtalyar, D. V.; Alpysbaeva, D. A.; Boinovich, L. B. *Colloids Surf. A* **2011**, *383*, 61.
19. Wang, P.; Qiu, R.; Zhang, D.; Lin, Z. F.; Hou, B. R. *Electrochim. Acta* **2010**, *56*, 517.
20. Zhang, F. Z.; Sun, M.; Xu, S. L.; Zhao, L. L.; Zhang, B. W. *Chem. Eng. J.* **2008**, *141*, 362.
21. Wang, P.; Zhang, D.; Qiu, R.; Hou, B. R. *Corros. Sci.* **2011**, *53*, 2080.
22. Liu, H. Q.; Szunerits, S.; Xu, W. G.; Boukherroub, R. *ACS Appl. Mater. Interf.* **2009**, *1*, 1150.
23. He, T.; Wang, Y. C.; Zhang, Y. J.; Lv, Q.; Xu, T. G.; Liu, T. *Corros. Sci.* **2009**, *51*, 1757.
24. (a) Qiu, R.; Zhang, D.; Wang, P. *Corros. Sci.* **2013**, *66*, 350. (b) Bocquet, L.; Lauga, E. *Nat. Mater.* **2011**, *10*, 334.
25. Herrasti, P.; Kulak, A. N.; Bavykin, D. V. *Electrochim. Acta* **2011**, *56*, 1323.
26. Wong, T. S.; Kang, S. H.; Tang, S. K. Y. *Nature* **2011**, *477*, 443.
27. Kim, P.; Wong, T. S.; Alvarenga, J. *ACS Nano* **2012**, *6*, 6569.
28. Epstein, A. K.; Wong, T. S.; Belisle, R. A.; Boggs, E. M.; Aizenberg, J. *Proc. Natl. Acad. Sci. U. S. A.* **2012**, *109*, 13182.
29. Lu, G.; Li, C.; Shi, G. *Polymer* **2006**, *47*, 1778.
30. Qiu, R.; Zhang, D.; Wang, P. *Electrochim. Acta* **2012**, *81*, 112.
31. Qiu, R.; Zhang, D.; Wang, P.; Zhang, X. L.; Kang, Y. S. *Electrochim. Acta* **2011**, *58*, 699.
32. Popov, K. I.; Djokic, S. S.; Grgur, B. N. Fundamental Aspects of Electrometallurgy; New York, **2002**.
33. Chougule, M. A.; Pawar, S. G.; Godse, P. R. *Soft Nanosci. Lett.* **2011**, *1*, 6.
34. Partch, R. E.; Gangolli, S. G.; Matijević, E.; Cal, W.; Arajs, S. *J. Colloid Interf. Sci.* **1991**, *144*, 27.
35. Ouyang, J. Y.; Li, Y. F. *Polymer* **1997**, *38*, 3997.
36. Azioune, A.; Chehimi, M.; Miksa, B.; Basinska, T.; Slomkowski, S. *Langmuir* **2002**, *18*, 1150.
37. Wenzel, R. N. *Ind. Eng. Chem.* **1936**, *28*, 988.
38. Arora, K.; Chaubey, A.; Singhal, R. *Biosens. Bioelectron.* **2006**, *21*, 1777.